Prospects of Kinetic Inductance Current Sensors for Multiplexed Microcalorimeter Readout

Galen C. O'Neil, Simon R. Bandler, Ian Fogarty Florang, John A. Mates, Daniel S. Swetz, Thomas R. Stevenson, Leaf A. Swordy, Joel N. Ullom, Michael R. Vissers, Jordan D. Wheeler, Wonsik Yoon, and Paul Szypryt

***Abstract*—Superconducting microcalorimeter arrays with hundreds to thousands of pixels are enabling new measurements and capabilities in exotic atom spectroscopy, X-ray astronomy, nuclear materials analysis, and many other fields. We consider the prospects of multiplexing microcalorimeters with the kinetic inductance current sensor (KICS), an alternative to the superconducting quantum interference device (SQUID) historically used to read out cryogenic microcalorimeters. We show that the amplifier-limited noise of the KICS is determined by its dynamic range, which is a free design parameter and tuneable with a DC current bias. We predict that KICS can meet the requirements to read out prototype metallic magnetic calorimeter pixels designed for the Lynx X-ray satellite mission concept with the use of low-latency tone tracking. We propose a KICS design that has both high coupling efficiency and high isolation between the RF and DC components of the circuit. We argue that the KICS provides engineering tradeoffs that are better suited to the readout of microcalorimeters when compared to the analogous microwave SQUID multiplexer.**

***Index Terms*—Kinetic inductance current sensor (KICS), magnetic microcalorimeter, microcalorimetes, multiplexing, superconducting resonator.**

I. Introduction

Superconducting microcalorimeter arrays with hundreds to thousands of pixels are enabling new measurements and capabilities in exotic atom spectroscopy, X-ray astronomy, nuclear materials analysis, and many other fields [1], [2], [3], [4]. These sensors provide a valuable combination of high detection efficiency and energy-resolving power. The detection efficiency is particularly high with very large arrays, and it is often desirable to read out these sensors with a multiplexing method, that is, to read out many sensors per amplifier channel. Microcalorimeter multiplexing has been developed and implemented using superconducting quantum interference devices (SQUIDs) through a variety of architectures, including time-division multiplexing [5], [6], frequency-division multiplexing [7], and microwave SQUID multiplexing (μMUX) [8], [9], [10] with impressive results [11]. Multiplexing methods ideally can be applied to many microcalorimeter technologies, including the transition-edge sensor (TES) [12], metallic magnetic microcalorimeter (MMC) [13], magnetic penetration depth thermometer [14], and even the recently developed λ-SQUID [15].

Recently, we demonstrated the readout of a TES-based visible to near-infrared single photon detector through a kinetic inductance current sensor (KICS) [16]. This result was impressive because the microcalorimeter was much faster than other microcalorimeters that have been successfully multiplexed. The pulse decay time of this detector was on order 1 μs, whereas SQUID multiplexers typically have sampling periods of a few microseconds, making them incompatible with such a fast microcalorimeter. An energy resolution comparable to or better than nonmultiplexed SQUID readout was achieved. We hope the reader of this article will leave understanding why the KICS was well suited to read out this very fast TES, and why the KICS is promising for other types of microcalorimeters that have historically been challenging to multiplex.

In this article, we describe the working principles of the KICS and derive the amplifier-limited noise of the KICS. We consider the use of the KICS for multiplexing other microcalorimeter systems that have so far been challenging with existing methods, namely, hydra MMCs developed for the Lynx X-ray satellite mission concept [17]. These hydra devices use thermal multiplexing to read out 25 spatial pixels with a single thermal sensor and have fairly demanding multiplexer requirements [18], [19]. The Lynx array design is very ambitious, aiming to use a combination of thermal and electronic multiplexing to simultaneously read out 100 000 pixels. We show that with low-latency tone-tracking, it is plausible to meet the Lynx multiplexing requirements with KICS devices very similar to the one used to read out the visible to near-infrared TES. We propose a readout circuit that combines high coupling efficiency with high RF isolation, well suited for coupling microcalorimeters to KICS readouts. Finally, we compare the KICS to the similar microwave SQUID multiplexer and argue that the KICS is particularly well suited to microcalorimeter applications because the KICS essentially trades off low-frequency noise performance for increased readout bandwidth.

Received 11 August 2025; revised 22 January 2026; accepted 3 March 2026. Date of publication 12 March 2026; date of current version 10 April 2026. This work was supported by the NASA under Grant NNH23OB118A, Grant 80NSSC23K0616, and Grant 80NSSC25K7636. *(Corresponding author: Galen C. O'Neil.)*

Galen C. O'Neil, John A. Mates, Daniel S. Swetz, Joel N. Ullom, Michael R. Vissers, and Jordan D. Wheeler are with the National Institute of Standards and Technology, Boulder, CO 80305 USA (e-mail: galen.oneil@nist.gov).

Simon R. Bandler, Thomas R. Stevenson, and Wonsik Yoon are with NASA Goddard Space Flight Center, Greenbelt, MD 20771 USA.

Ian Fogarty Florang, Leaf A. Swordy, and Paul Szypryt are with the National Institute of Standards and Technology, Boulder, CO 80305 USA, and also with the University of Colorado, Boulder, CO 80305 USA.

Color versions of one or more figures in this article are available at https://doi.org/10.1109/TASC.2026.3673656.

Digital Object Identifier 10.1109/TASC.2026.3673656

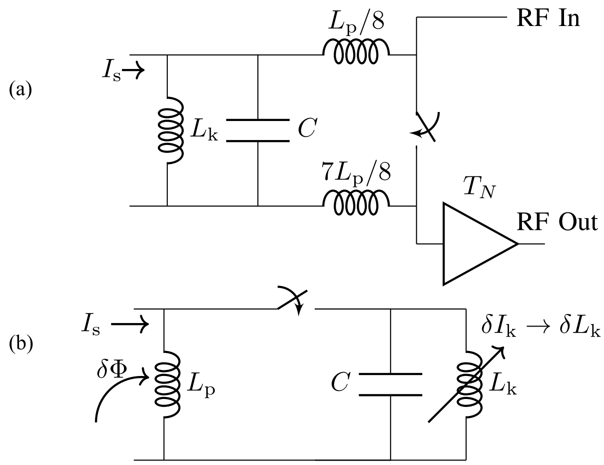

Fig. 1. (a) Circuit model for the baseline KICS. A superconducting LC resonator with capacitor C and asymmetric inductive coupling to an RF feedline with inductance L_p forming a loop with kinetic inductance element L_k. The transmitted RF power is amplified by an amplifier with noise temperature T_N. The device was used to measure input current I_s from a TES. Persistent current is trapped by a switch consisting of a portion of the superconducting feedline with lower superconducting transition temperature. For the baseline KICS, DC current to be trapped was applied via the RF feedline using a bias tee before and after the sample chip. (b) Generalized circuit model of a directly coupled KICS resonator. Although coupling to an RF transmission line is required for readout, it is not shown here for simplicity and generality (inductive versus capacitive coupling). Inductance L_{p} is required to complete the persistent current loop, which provides bias current I_{b}. The resonant frequency of the KICS is sensitive to current I_{s} or applied flux $\delta\Phi$ because each induces a change in current I_{k} through the kinetic inductance element. An external magnetic field coil or additional DC leads may be used to facilitate trapping the required persistent current.

II. Working Principles of KICS and Amplifier Limited Noise

A KICS consists of a nonlinear kinetic inductance element biased with a persistent superconducting loop current I_{b} and embedded in a resonant circuit, which is coupled to a microwave transmission line. Kinetic inductance arises from the kinetic energy of the current carrying Cooper pairs. In disordered superconductors with a large kinetic inductance fraction, the kinetic inductance has a nonlinear current dependence

$$L_{\mathrm{k}}(I_{\mathrm{k}}) = L_{\mathrm{k}}(0)\left[1 + (I_{\mathrm{k}}^2/I_*^2) + \cdots\right] \tag{1}$$

where $L_{\mathrm{k}}(I_{\mathrm{k}})$ is the kinetic inductance at current I_{k}, and I_* is the characteristic current scale of the nonlinearity [20]. The persistent bias current I_{b} sets the current sensitivity without coupling to an external bias circuit during regular operation, which may otherwise result in excess noise. Any additional input current, such as from a microcalorimeter being read out, will shift the resonant frequency. Many KICS devices coupled to a single RF transmission line may be read out in much the same way as kinetic inductance detectors [21], [22] and μMUX readouts [8], [9], [10].

We begin by analyzing the noise of the KICS used to read out the optical TES, which we will refer to as the *baseline* KICS. A circuit model for this device is shown in Fig. 1(a). We will analyze the behavior of the KICS using the simplified KICS resonator in Fig. 1(b). When coupled to an RF transmission line the forward transmission coefficient is

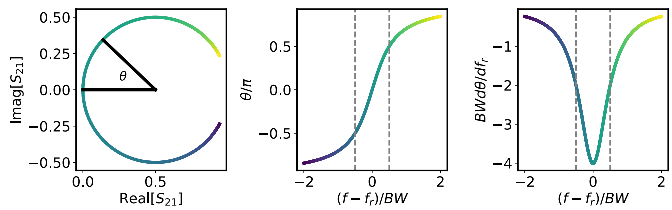

Fig. 2. Response of a feed line coupled resonator with coupling-limited bandwidth. *(Left)* The real and imaginary components of S_{21} and the arc angle θ. The noise on the arc angle *(Middle)* θ as a function of detuning. *(Right)* The arc angle responsivity as a function of detuning. Vertical lines show detuning of positive and negative one half-bandwidth. The signal-to-noise ratio is reduced for large values of arc angle because, while the noise in arc angle is independent of detuning, the arc angle responsivity is reduced.

$$S_{21} = 1 - \frac{Q/Q_{\mathrm{c}}}{1 + 2iQ\frac{f_{\mathrm{r}}-f}{f_r}}. \tag{2}$$

where Q is the total quality factor, Q_{c} is the coupling quality factor, f is the readout tone frequency, and f_{r} is the resonant frequency. We assume a coupling-limited bandwidth, so $Q \approx Q_{\mathrm{c}}$ and the full-width half-maximum bandwidth is f/Q. The resonant frequency $f_{\mathrm{r}}(I_{\mathrm{k}}) \approx (2\pi\sqrt{L_{\mathrm{r}}(I_{\mathrm{k}})C})^{-1}$, where $L_{\mathrm{r}}(I_{\mathrm{k}})$ is the effective inductance of the resonant circuit. When a signal shifts a superconducting resonator by a sizable fraction of the bandwidth, it can be convenient to read out the signal using the arc angle θ, so we will analyze the noise in terms of this arc angle. Some relevant properties of S_{21}, including the definition of the arc angle, are shown in Fig. 2. When the resonator is probed with a fixed-frequency tone of power P_{feed} at the resonant frequency $f = f_{\mathrm{r}}(I_{\mathrm{b}})$, the amplifier with noise temperature T_{N} will contribute arc angle noise power [11]

$$S_\theta^{T_{\mathrm{N}}} \approx 4\frac{k_{\mathrm{B}}T_{\mathrm{N}}}{P_{\text{feed}}}. \tag{3}$$

The noise in arc angle is independent of detuning $(f - f_r)$. When the amplifier noise is the dominant white noise source the input referred current noise power is

$$S_{I_{\mathrm{s}}} \approx S_\theta^{T_{\mathrm{N}}}\left(\frac{d\theta}{dI_{\mathrm{s}}}\right)^{-2} = \frac{k_{\mathrm{B}}T_{\mathrm{N}}}{P_{\text{feed}}}I_{\mathrm{HW}}^2 \tag{4}$$

where we use the relation

$$\frac{d\theta}{dI_{\mathrm{s}}} = \frac{d\theta}{df_{\mathrm{r}}}\frac{df_{\mathrm{r}}}{dI_{\mathrm{s}}} = \frac{4Q}{f}\frac{f}{2QI_{\mathrm{HW}}} = \frac{2}{I_{\mathrm{HW}}} \tag{5}$$

and where I_{HW} is the current required to shift the resonator frequency by one half-bandwidth and assuming a linear relationship between f_r and I_s over the range of a bandwidth of frequency shift. We shall refer to maximum signal size that may be read out without degradation as the dynamic range, and the dynamic range is proportional to I_{HW}.

The baseline KICS had $Q_{\mathrm{c}} = 1.1\times10^3$, $I_{\mathrm{HW}} = 1.8\,\mu\mathrm{A}$, and $f_r = 4.0\,\mathrm{GHz}$ at $I_{\mathrm{b}} = 2.0\,\mathrm{mA}$. When operated with $P_{\text{feed}} = 100\,\mathrm{pW}(-70\,\mathrm{dBm})$, we measured $\sqrt{S_{\mathrm{I}}} = 1.4\,\mathrm{pA}/\sqrt{\mathrm{Hz}}$ in the signal free dissipation quadrature, which equates to $T_{\mathrm{N}} \approx 4\,\mathrm{K}$ and is consistent with typical observed HEMT amplifier noise values.

The kinetic inductance element must be in parallel with an inductance L_p in order to trap a persistent current. In the directly coupled KICS circuit model [see Fig. 1(b)], the resonant frequency is sensitive to the parallel inductance $L_\mathrm{r} = \frac{L_\mathrm{k}L_\mathrm{p}}{L_\mathrm{k}+L_\mathrm{p}}$, while input current I_s sees an inductive current splitter such that $\frac{dI_\mathrm{k}}{dI_\mathrm{s}} = \frac{L_\mathrm{p}}{L_\mathrm{p}+L_\mathrm{k}}$, we are assuming the input signal is slow enough that we may neglect the capacitance. These relations suggest that greater sensitivity is achieved when $L_\mathrm{p} \gg L_\mathrm{k}$. We relate the key parameters affecting the noise to the circuit and material parameters using the chain rule

$$\frac{df_\mathrm{r}}{dI_\mathrm{s}} = \frac{df_\mathrm{r}}{dL_\mathrm{r}}\frac{dL_\mathrm{r}}{dL_\mathrm{k}}\frac{dL_\mathrm{k}}{dI_\mathrm{k}}\frac{dI_\mathrm{k}}{dI_\mathrm{s}}. \tag{6}$$

Using the directly coupled KICS circuit model in Fig. 1(b) and (1), we find $\frac{df_\mathrm{r}}{dL_\mathrm{r}} = \frac{-f_\mathrm{r}}{2L_\mathrm{r}}$, $\frac{dL_\mathrm{r}}{dL_\mathrm{k}} = \frac{L_\mathrm{p}^2}{(L_\mathrm{k}+L_\mathrm{p})^2}$, and $\frac{dL_\mathrm{k}}{dI_\mathrm{k}} = \frac{2L_\mathrm{k}I_\mathrm{b}}{I_*^2}$, keeping the lowest order term in (1). In the baseline KICS, $L_\mathrm{p} = 8\,\mathrm{nH}$ and $L_\mathrm{k}(0) = 1\,\mathrm{nH}$.

Both the noise and the dynamic range of a KICS readout are set by I_HW, then we find

$$I_\mathrm{HW} = \frac{1}{2Q}\frac{(L_\mathrm{k}+L_\mathrm{p})^2}{L_\mathrm{p}^2}\frac{I_*^2}{I_\mathrm{b}}. \tag{7}$$

For a device with a given bandwidth (set by Q) and characteristic current scale I_*, the noise is minimized when the bias current I_b is maximized. The noise may be further decreased by reducing I_*, which is predicted to scale with the cross-sectional area of the kinetic inductance element [20]. Since both I_* and the maximum usable value of I_b are proportional to critical current, the ratio I_*/I_b can be considered constant for a given material, and $I_\mathrm{HW} \propto I_*$. The baseline KICS used a NbTiN kinetic inductance element that was 20 nm thick and 700 nm wide, while NbTiN superconducting nanowire sensors are regularly fabricated with 7 nm thickness and 70 nm width [23]. The kinetic inductance nonlinearity of NbTiN has previously been characterized at thicknesses as low as 4 nm [24]. Beware, a small kinetic inductance element will act like a superconducting nanowire sensor and will lose its trapped current if sufficient energy is deposited by a photon or other particle. Increasing I_HW is easy with larger cross-sectional kinetic inductance elements, reduced I_b, or reduced coupling to the signal source. Based on this, I_HW may be varied in the range of 30× lower to arbitrarily larger than in the baseline KICS while maintaining the same quality factor. Both the dynamic range and noise of a KICS device are determined by I_HW, which is easily controlled over a wide range of values and may be considered a design parameter.

III. Flux Sensitive KICS and Energy Sensitivity

A KICS is also flux sensitive when a flux signal induces a change in the current I_k, with an amplifier-limited flux noise power

$$S_\Phi = S_\theta^{T_\mathrm{N}}\left(\frac{d\theta}{d\Phi}\right)^{-2} \approx \frac{k_\mathrm{B}T_\mathrm{N}}{P_\mathrm{feed}}\Phi_\mathrm{HW}^2. \tag{8}$$

Flux sees the inductance of the persistent current loop in series such that $L_\mathrm{s} = \frac{d\Phi}{dI_\mathrm{k}} = L_\mathrm{k} + L_\mathrm{p}$, and the flux change for a half-bandwidth shift is $\Phi_\mathrm{HW} \approx L_\mathrm{s}I_\mathrm{HW}$. Since I_HW is a design parameter, Φ_HW is also a design parameter. The performance of a SQUID for MMC readout is often characterized by the energy sensitivity, ε_K [25]. We evaluate the KICS using the same metric, replacing the SQUID inductance with the series KICS inductance

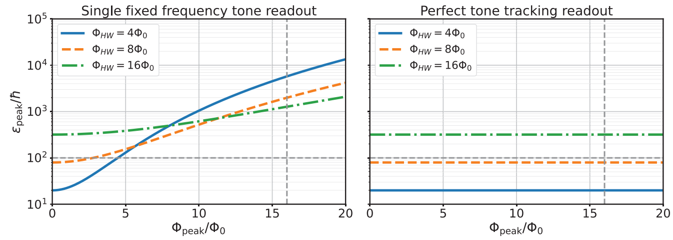

Fig. 3. *(Left)* Predicted energy sensitivity at the peak of a pulse for single tone readout versus Φ_peak for various values of Φ_HW. The vertical dashed line shows a Φ_peak based on Lynx prototype MMC pixels and the mission energy range, and the horizontal dashed line shows energy sensitivity required for the readout of the Lynx pixels. *(Right)* The same with a perfect tone-tracking readout.

$$\varepsilon_\mathrm{K} = \frac{S_\Phi}{2L_\mathrm{s}} \approx \frac{k_\mathrm{B}T_\mathrm{N}}{2L_\mathrm{s}P_\mathrm{feed}}\Phi_\mathrm{HW}^2. \tag{9}$$

Many MMC applications, including the proposed Lynx MMC X-ray spectrometer, require $\varepsilon_\mathrm{K} \approx 100\hbar$, while the best nonmultiplexed DC SQUID readouts approach $\varepsilon_\mathrm{K} \approx 10\,\hbar$[13], [18], [25]. We calculate $\varepsilon_\mathrm{K} = 80\hbar$ for the baseline KICS with $\Phi_\mathrm{HW} = 8\Phi_0$, where Φ_0 is the flux quantum.

IV. Can a KICS Read Out a Lynx MMC Hydra Pixel?

This initial finding of a desirably low energy sensitivity is encouraging, but we must consider the dynamic range of the KICS compared to the signal size. All superconducting resonators have a drop in responsivity when detuned away from the deepest part of the resonance; in the right panel of Fig. 2, we can see that $\frac{d\theta}{df_\mathrm{r}}$ is reduced to half the maximum value at one half-bandwidth shift. Therefore, the flux noise during a pulse is nonstationary and worse for large pulses. Fig. 3 (left) shows predicted energy sensitivity at the peak of a pulse of height Φ_peak for various values of Φ_HW and otherwise identical parameters to the baseline KICS with fixed frequency readout, as well as the peak signal size for a Lynx MMC pixel. For a concrete comparison, we use the signal size for a Lynx prototype MMC hydra pixel with a $0.8\,\mu\mathrm{m}$ meander [19], which has pickup coil inductance of 6.3 nH fairly close to the baseline KICS parallel inductance of 9 nH. This prototype Lynx MMC has a maximum signal size of $16\Phi_0$ at the high end of the target energy range for the Lynx spectrometer, and the rise time is about 5 μs. No choice of Φ_HW achieves the required energy sensitivity at the peak of the pulse for fixed frequency readout and noise temperature 4 K.

Tone-tracking is a digital feedback method that updates the frequency of the readout tone to minimize detuning during a pulse. By minimizing detuning, the flux noise is reduced for large pulses. Fig. 3 (right) shows that with perfect zero-latency tone-tracking, the Lynx MMC sensitivity requirement is easily met. Real tone-tracking will have finite latency. The SLAC Microresonator RF (SMURF) electronics platform implements tone-tracking for a microwave SQUID readout with 8.8 μs

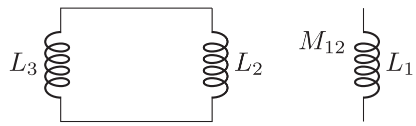

Fig. 4. Inductive impedance transformer consisting of inductor L_1 coupled by a mutual inductance M_{12} to L_2, which is in parallel with L_3. For appropriate choices of the component values, the effective inductance is $\sim L_3$.

latency and the developers identify the use of a polyphase filter bank algorithm for tone generation as the largest source of latency [26]. Tones may be generated with lower latency with other algorithms, typically at the cost of additional field programmable gate array resources, reducing the largest source of latency. Other sources of latency will be harder to reduce and will likely determine the minimum achievable tone-tracking latency; the SMURF paper reports a 100 ns cable delay and 500 ns digital-to-analog and analog-to-digital conversion latencies [26]. The tone-tracking latency required for a given application will be of order $\tau_{\rm rise}\Phi_{\rm detune}/\Phi_{\rm peak}$, where $\tau_{\rm rise}$ is the signal rise time and $\Phi_{\rm detune}$ is the maximum acceptable detuning expressed in flux units. We estimate $\Phi_{\rm detune} = 4\Phi_0$ for a KICS with $\Phi_{\rm HW} = 4\Phi_0$ based on the point where the energy sensitivity trace crosses the requirement line in Fig. 3 (left). Therefore, we predict that a tone-tracking latency of 1.25 μs may be sufficient to meet the Lynx MMC sensitivity requirement for a pixel with a rise time of 5 μs, without needing to improve the amplifier noise temperature.

The energy sensitivity of the KICS readout may be improved, or the tone-tracking latency requirement may be relaxed, by using an amplifier with a lower noise temperature. Quantum-limited parametric amplifiers based on kinetic inductance with noise temperature well below semiconductor amplifiers are being developed for many quantum applications [20], [27]. These amplifiers may be particularly well matched to the KICS because 1) these amplifiers are commonly made from NbTiN to achieve nonlinear kinetic inductance, opening up the possibility of cofabrication with KICS sharing the kinetic inductance layer, and 2) these amplifiers tend to have lower saturation powers than HEMTs so they will work better in the presence of tone-tracking, which limits the power reaching the amplifier.

V. RF Nulling KICS

Every element coupled to a superconducting resonator has the potential to introduce undesired loss and/or parasitic resonances. It is therefore desirable to limit the number of circuit elements that have RF coupling and especially to limit RF coupling to the microcalorimeter being read out. We propose the *RF nulling KICS* that allows for nearly optimal signal coupling efficiency and zero RF coupling to the microcalorimeter to be read out. The baseline KICS made use of a resistive low-pass filter to provide RF isolation. However, the Johnson noise from this filter significantly exceeded the KICS readout noise, therefore the filter is not a good solution for all readout applications, and it is particularly poorly matched to MMC readout.

The inductive impedance transformer (see Fig. 4) has the property that effective inductance depends on the magnitude of the mutual inductance, while the voltage across the kinetic inductance (L_3) depends on the sign of the mutual inductance. The mutual inductance $M_{12} = k\sqrt{L_1 L_2}$ is bounded by the coupling efficiency $0 \le |k| \le 1$. For $L_3 \ll L_2 = L_1$ and $|k| = 1$, the effective inductance of the whole circuit is L_3. Here, effective inductance is defined such that $V_1 = L_{\rm eff}\frac{dI_1}{dt}$, where V and I refer to the voltage across and current through the inductor with the same subscript.

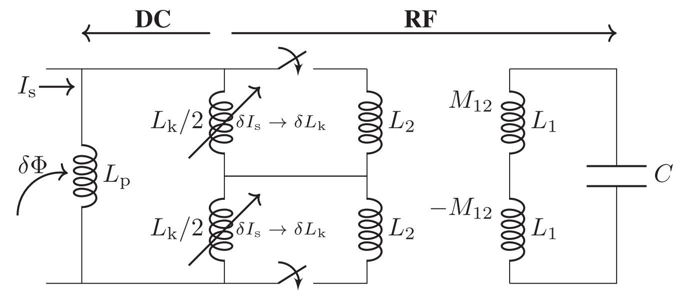

Fig. 5. Proposed RF nulling KICS circuit. Two connected inductive impedance transformers in series provide effective inductance $L_{\rm k}$, where the two loops on the left share a connecting wire. The RF contribution to voltage $V_{\rm p}$ across the inductance $L_{\rm p}$ is equal to zero because the voltages $V_{\rm k}$ across the two kinetic inductance elements $L_{\rm k}$ are equal and opposite. The circuit has two persistent current loops, which can be biased with currents $I_{\rm b}$ of equal sign and magnitude. If the two persistent currents were individually adjustable, they could be used to fine tune the RF nulling to account for fabrication variation. The flux coupling efficiency can be comparable to a directly coupled KICS.

The RF nulling KICS in Fig. 5 uses two such transformers with mutual inductance of opposite sign. The effective inductance depends on the magnitude of the mutual inductance and sums to the inductance of two kinetic inductance elements in series. The RF voltage across the kinetic inductance elements depends on the sign of the mutual inductance and ideally sums to zero, eliminating all RF coupling to the DC portion of the circuit.

We analyze the lumped element RF nulling KICS circuit model to determine the effect of nonuniform inductance values on the RF isolation. The approach is to introduce a parameter y representing the unequal inductance values and a resistor R in parallel with L_p, then choose the resistance to have value $R_{\rm opt}$ to maximize loss, and finally, we calculate the minimum quality factor $Q_{\rm min}$ due to the DC portion of the circuit. We find the total impedance measured across the capacitor is

$$Z_{\rm total} = \frac{1}{j\omega C} + j\omega L_{\rm base} + \frac{\omega^2 M_{\rm net}^2}{\frac{j\omega L_p R}{R + j\omega L_p} + j\omega L_{\rm sec}} \tag{10}$$

where the transformed kinetic inductance is

$$L_{\rm base} = \left(L_1 - \frac{M_{12}^2}{L_2 + L_3(1+y)}\right) + \left(L_1 - \frac{M_{12}^2}{L_2 + L_3(1-y)}\right) \tag{11}$$

where L_3 is the mean value and $2y$ is the fractional difference of the values of the two kinetic inductance elements, the net effective mutual inductance

$$M_{\rm net} \approx 2M_{12}y\frac{L_2 L_3}{(L_2 + L_3)^2} \tag{12}$$

TABLE I
COMPARISON OF KICS TO μMUX WITH AND WITHOUT FRM

	KICS	**μMUX without FRM**	**μMUX with FRM**
$\frac{\text{Resonator Bandwidth}}{\text{Readout Bandwidth}}$ ratio	1	1	2–32
Low-frequency noise	TLS limited	TLS limited	Modulated away
High-frequency noise	No penalty	No penalty	FRM penalty
Responsivity nearly independent of quiescent detector current	Yes	No	Yes

is proportional to y, the series inductance of the two transformers is

$$L_{\text{sec}} = \frac{L_2 L_3(1+y)}{L_2 + L_3(1+y)} + \frac{L_2 L_3(1-y)}{L_2 + L_3(1-y)} \approx \frac{2L_2 L_3}{L_2 + L_3} \tag{13}$$

and $j = \sqrt{-1}$. The quality factor

$$Q = \frac{\omega_0 L_{\text{eff}}}{\text{Re}(Z_{\text{total}})} \tag{14}$$

is minimized when we maximize $\text{Re}(Z_{\text{total}})$, and we find R_{opt}

$$R_{\text{opt}} = \omega \frac{L_{\text{sec}} L_p}{L_{\text{sec}} + L_p}. \tag{15}$$

At the point of maximum loss ($R = R_{\text{opt}}$), the resonant frequency ω_0 is found by solving $\text{Im}(Z_{\text{total}}) = 0$. We find the resonant frequency

$$\omega_0 = \frac{1}{\sqrt{C L_{\text{eff}}}} \tag{16}$$

where

$$L_{\text{eff}} = L_{\text{base}} - \frac{M_{\text{net}}^2 (L_p + 2L_{\text{sec}})}{2L_{\text{sec}}(L_p + L_{\text{sec}})} \tag{17}$$

and as expected that the resonant frequency is independent of the DC portion when y and therefore M_{net} are zero. The minimum quality factor due to the DC portion of the circuit is

$$Q_{\text{min}} = \frac{\omega_0 L_{\text{eff}}}{\text{Re}(Z_{\text{total}})|_{R=R_{\text{opt}}}} = \frac{2L_{\text{eff}} L_{\text{sec}}(L_{\text{sec}} + L_p)}{M_{\text{net}}^2 L_p}. \tag{18}$$

Using the approximation $L_{\text{eff}} \approx \frac{1}{\omega_0^2 C}$ and substituting in the circuit parameters

$$Q_{\text{min}} = \frac{1}{\omega_0^2 C M_{12}^2 y^2} \frac{(L_2 + L_3)^3}{L_2 L_3} \left(1 + \frac{2L_2 L_3}{L_p(L_2 + L_3)}\right). \tag{19}$$

For component values similar to the baseline KICS ($L_1 = L_2 = M_{12} = L_p = 10$ nH, $L_3 = L_k/2 = 0.5$ nH, $f_0 = 4$ GHz, and $C = 1.62$ pF), we find that $y = 0.016$ results in $Q_{\text{min}} = 10^4$, which is much greater than the coupled quality factor of 1.1×10^3. The analysis and result are very similar for unequal mutual inductance.

The RF nulling KICS effectively divides the circuit into an RF and DC portion while maintaining the possibility of high coupling efficiency. Lumped element circuit analysis shows that an RF nulling KICS with parameters similar to the baseline KICS can tolerate inductance and mutual inductance nonuniformity of order 1% . Fabrication-based imbalance in inductance would come primarily from variation in dimension, variation in dimensions is minimized when fabricated elements are close to each other, like these elements would be, so 1% level matching is likely not very difficult to achieve. A similar approach to RF nulling will likely work for microwave SQUID multiplexers as well.

VI. KICS Compared to Microwave μMUX

Both KICS and μMUX [11], [28] readouts are based on dissipationless superconducting resonators in which input signal is transduced to a change in resonant frequency. The amplifier-limited noise in both devices follows (3). Other considerations, such as the optimal readout power, crosstalk, limits of room temperature electronics, and the effects of finite internal quality factors, are similar between the two devices. Here we consider the differences between the two devices for the purposes of microcalorimeter readout.

The fundamental difference between KICS and μMUX is the nature of the response function. KICS has a monotonic response function (1), while μMUX has a periodic response function. Flux ramp modulation (FRM) is used in most μMUX systems to linearize the signal and avoid the $1/f$ two-level system (TLS) noise that exists in all superconducting resonators and is particularly significant at low frequencies [29]. FRM uses the periodic response of the SQUID plus a linear ramp to modulate the resonant frequency as $f_{\text{r}}(t) \approx \sin(rt + s)$, where r is the input flux ramp rate, t is time, s is the signal, and sin approximates the response of the SQUID. With FRM, the signal s appears as a phase and is read out at a speed between $2\times$ (Nyquist limit for small signals) and $16\times$ to $32\times$ (commonly implemented) slower than the arc angle is read out. There is a noise penalty in FRM because the SQUID is in an insensitive region of the response function half of the time [11]. While μMUX can operate without FRM, the responsivity is maximized only when each SQUID is biased to the steepest portion of its response, which is nontrivial to ensure for an array of devices with typical variations in quiescent currents. On the other hand, the KICS does not modulate signals away from $1/f$ TLS noise, as is the case with the μMUX FRM. However, the TLS may not be a major issue for some microcalorimeter applications as the $1/f$ knee in the baseline KICS was about 1 kHz, sufficiently low that it would not increase the noise in the Lynx MMC signal bandwidth of 10 to 20 kHz. Nevertheless, there are methods for reducing TLS noise by limiting electric fields in lossy materials [29], [30].

Table I summarizes the differences between KICS and μMUX with and without FRM. μMUX gives up readout bandwidth to gain excellent low-frequency noise, while KICS gives up low-frequency performance to gain readout bandwidth.

Some microcalorimeter applications will benefit from the KICS tradeoff because microcalorimeter signals often have a steep rising edge with high slew rate and significant information content at higher frequencies.

VII. Conclusion

In this article, we analyze the amplifier-limited noise of the KICS and find that both the noise and dynamic range are set by the current required to shift the resonator by one half-bandwidth, which can be varied over a wide range of values. We find that KICS combined with low-latency tone-tracking is a promising path toward meeting the challenging requirements for the readout of hydra MMC pixels designed for the Lynx X-ray satellite mission concept. We propose an RF nulling circuit to limit RF coupling to the devices read out by KICS. Finally, we argue that KICS gives up low-frequency performance for increased readout bandwidth when compared to μMUX with FRM, which can be a favorable tradeoff for many microcalorimeter applications.

References

[1] K. E. Koehler, "Low temperature microcalorimeters for decay energy spectroscopy," *Appl. Sci.*, vol. 11, 2021, Art. no. 4044.

[2] T. Y. Saito et al., "Application of hard X-ray and gamma-ray TES microcalorimeter at accelerator facility," *IEEE Trans. Appl. Supercond.*, vol. 35, no. 5, pp. 1–5, Aug. 2025.

[3] J. P. Smith, B. A. Mazin, A. Boaventura, K. J. Thompson, and M. Daal, "Improved flexible coaxial ribbon cable for high-density superconducting arrays," *IEEE Trans. Appl. Supercond.*, vol. 34, pp. 1–6, Mar. 2024.

[4] P. Szypryt et al., "A transition-edge sensor-based X-ray spectrometer for the study of highly charged ions at the national institute of standards and technology electron beam ion trap," *Rev. Sci. Instrum.*, vol. 90, 2019, Art. no. 123107.

[5] W. B. Doriese et al., "Developments in time-division multiplexing of X-ray transition-edge sensors," *J. Low Temp. Phys.*, vol. 184, pp. 89–395, 2015.

[6] D. Vaccaro et al., "System performance of a cryogenic test-bed for the time-division multiplexing readout for the newathena X-ray integral field unit," *J. Astron. Telescopes Instrum. Syst.*, vol. 10, pp. 1–13, 2024.

[7] D. Vaccaro et al., "Developments on frequency domain multiplexing readout for large arrays of transition-edge sensor X-ray micro-calorimeters," *J. Low Temp. Phys.*, vol. 216, pp. 21–28, 2024.

[8] J. Mates, The microwave SQUID multiplexer. Ph.D. thesis, Univ. Colorado, Boulder, CO, USA, 2011.

[9] D. Richter et al., "Simultaneous MMC readout using a tailored μMUX based readout system," *IEEE Trans. Appl. Supercond.*, vol. 33, no. 5, Aug. 2023, Art. no. 2500705.

[10] O. Noroozian et al., "High-resolution gamma-ray spectroscopy with a microwave-multiplexed transition-edge sensor array," *Appl. Phys. Lett.*, vol. 103, 2013, Art. no. 202602.

[11] H. Akamatsu, W. B. Doriese, J. A. B. Mates, and B. D. Jackson, *Signal readout for transition-edge sensor X-ray imaging spectrometers*, 2023. [Online]. Available: https://link.springer.com/rwe/10.1007/978-981-16-4544-0_24-1

[12] K. D. Irwin, G. C. Hilton, and C. E. Ed, *Transition-Edge Sensors*. Berlin, Germany: Springer, 2005.

[13] S. Kempf, A. Fleischmann, L. Gastaldo, and C. Enss, "Physics and applications of metallic magnetic calorimeters," *J. Low Temp. Phys.*, vol. 193, pp. 365–379, 2018.

[14] T. R. Stevenson et al., "Superconducting effects in optimization of magnetic penetration thermometers for X-ray microcalorimeters," *IEEE Trans. Appl. Supercond.*, vol. 23, no. 3, Jun. 2013, Art. no. 2300605.

[15] C. Schuster and S. Kempf, "Squid-based superconducting microcalorimeter with in situ tunable gain," *Appl. Phys. Lett.*, vol. 123, 2023, Art. no. 252603.

[16] P. Szypryt et al., "Kinetic inductance current sensor for visible to near-infrared wavelength transition-edge sensor readout," *Commun. Eng.*, vol. 3, 2024, Art. no. 160.

[17] T. L. Team, "Lynx X-ray observatory concept study report," 2019. [Online]. Available: https://wwwastro.msfc.nasa.gov/lynx/docs/LynxConceptStudy.pdf

[18] T. R. Stevenson et al., "Magnetic calorimeter option for the Lynx x-ray microcalorimeter," *J. Astron. Telescopes Instrum. Syst.*, vol. 5, 2019, Art. no. 1.

[19] W. Yoon et al., "Design and performance of a prototype magnetic calorimeter array for the Lynx X-ray microcalorimeter," *IEEE Trans. Appl. Supercond.*, vol. 29, no. 5, 2019, Art. no. 2300206.

[20] B. H. Eom, P. K. Day, H. G. Leduc, and J. Zmuidzinas, "A wideband, low-noise superconducting amplifier with high dynamic range," *Nature Phys.*, vol. 8, pp. 623–627, 2012.

[21] P. K. Day, H. G. LeDuc, B. A. Mazin, A. Vayonakis, and J. Zmuidzinas, "A broadband superconducting detector suitable for use in large arrays," *Nature*, vol. 425, pp. 817–821, 2003.

[22] J. P. Smith, J. I. Bailey, A. Cuda, N. Zobrist, and B. A. Mazin, "MKIDGen3: Energy-resolving, single-photon-counting microwave kinetic inductance detector readout on a radio frequency system-on-chip," *Rev. Sci. Instrum.*, vol. 95, 2024, Art. no. 114705.

[23] S. Dong et al., "Establishing an end-to-end workflow for SNSPD fabrication and characterization," *Sci. Rep.*, vol. 14, pp. 1–11, 2024.

[24] A. Giachero et al., "Characterization of NbTiN films with thicknesses below 20 nm for low power kinetic inductance amplifiers," *IEEE Trans. Appl. Supercond.*, vol. 33, no. 5, Aug. 2023, Art. no. 1700905.

[25] A. Fleischmann et al., "Metallic magnetic calorimeters," *AIP Conf. Proc.*, vol. 1185, pp. 571–578, 2009.

[26] C. Yu et al., "SLAC microresonator RF (SMuRF) electronics: A tone-tracking readout system for superconducting microwave resonator arrays," *Rev. Sci. Instrum.*, vol. 94, 2023, Art. no. 014712.

[27] M. Malnou et al., "Performance of a kinetic inductance traveling-wave parametric amplifier at 4 Kelvin: Toward an alternative to semiconductor amplifiers," *Phys. Rev. Appl.*, vol. 17, 2022, Art. no. 1.

[28] M. Wegner et al., "Microwave squid multiplexing of metallic magnetic calorimeters: Status of multiplexer performance and room-temperature readout electronics development," *J. Low Temp. Phys.*, vol. 193, pp. 462–475, 2018.

[29] J. Gao, The physics of superconducting microwave resonators. Ph.D. thesis, California Inst. Technol., Pasadena, CA, USA, 2008.

[30] S. Ganjam et al., "Surpassing millisecond coherence in on chip superconducting quantum memories by optimizing materials and circuit design," *Nature Commun.*, vol. 15, 2024, Art. no. 3687.